Research Article | Vol. 26, No. 15 | 23 Jul 2018 | OPTICS EXPRESS 19614
Optics EXPRESS

Electro-wetting lenticular lens with improved diopter for 2D and 3D conversion using lens-shaped ETPTA chamber

JUNOH KIM, DOOSEUB SHIN, JUNSIK LEE, GYOHYUN KOO, CHEOLJOONG KIM, JEE HOON SIM, GYUSUK JUNG, AND YONG HYUB WON*

School of Electrical Engineering, Korea Advanced Institute of Science and Technology, Daejeon 34141, South Korea
**yhwon@kaist.ac.kr*

Abstract: In this paper, we introduce a method for improving the lens diopter of 2D/3D convertible devices using electro-wetting. For stable operation, an electro-wetting device requires high dioptric performance and this was achieved using bi-convex liquid-liquid-solid phases. 1-Chloronaphthalene with a refractive index of 1.633 was used as an oil phase to achieve high diopters. ETPTA (trimethylolpropane ethoxylate triacrylate), a UV-sensitive material with low chemical reactivity to the 1-Chloronaphthalene, was used as a chamber material. This resulted in a diopter of 3030D for high quality multi-view images without unstable oil movement or trembling. The ETPTA was molded on a 0.3mm thick glass substrate that was coated with UV adhesive (NOA 81). The maximum diopter capable of stable operation was 3425D. 2D and 3D conversion and parallax motion were demonstrated.

1. Introduction

3D displays are in great demand, and although various studies are underway, they have not yet achieved the technological advancements that would allow them to enter the market. One of the most realistic approaches for generating the 3D effect is to use multi-view displays [1]. At present, there are two different types of multi-view. One is based on a parallax barrier [2–5] and the other is lenticular in design [6–8]. Although the parallax barrier method has advantages in terms of easier process and design, it has the disadvantage of decreased brightness depending on the number of viewpoints.

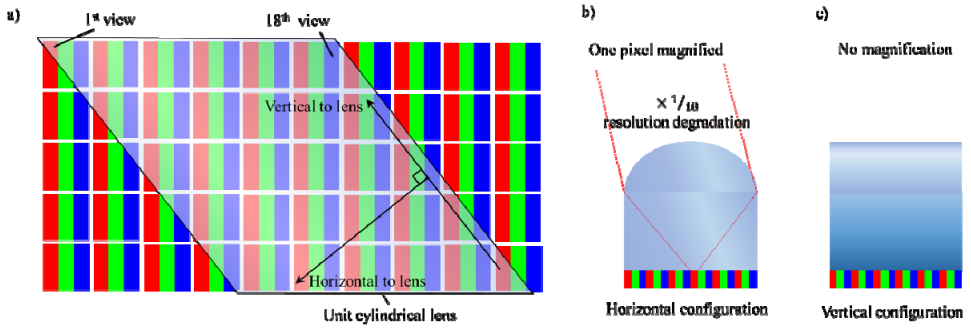

Fig. 1. (a) A layout structure between a lens and pixels and (b) in the horizontal configuration with 18 times magnification and (c) the vertical configuration with no magnification.

However, designing a lenticular system is more difficult than the parallax barrier method [9]. More specifically, the lenticular approach can be powerful, but only if the initial design is good.

The most difficult factor in a multi-view system is 3D resolution. To observe natural 3D motion parallax in a multi-view system, multiple viewpoints are required. However, the

#332838 https://doi.org/10.1364/OE.26.019614
Journal © 2018 Received 30 May 2018; revised 11 Jul 2018; accepted 13 Jul 2018; published 19 Jul 2018

Optics EXPRESS

number of viewpoints is in a trade-off relationship with 3D resolution. The number of viewpoints may be increased as the number of pixels included in one lens increases.

For any particular display, the 3D resolution will ultimately be determined by the size of the one cylindrical lens that makes up the lenticular component. Generally, the 3D resolution of a display having more than 18 viewpoints is lower than VGA (Video Graphics Array, 800 by 600 resolution) grade when the background display is UHD (Ultra High Definition, 3840 by 2160 resolution) grade, since the 3D resolution is reduced 18 times in the horizontal direction of the lens. Figure 1 shows the horizontal and the vertical configurations of the unit lens. In markets that are accustomed to high resolution, it may not be possible to enjoy all types of content with such low resolution. In practice, people may require a device that is switchable between 2D and 3D functions. With this in mind, many studies are underway to realize a 2D/3D convertible device.

To achieve 2D/3D conversion, several liquid crystal methods have been used to form a separate lens state and flat state [10,11], and in another approach, hydrostatic pressure was applied to flexible membranes [12]. However, since liquid crystals use the index difference of the polymer and the liquid crystal, and are sensitive to cell gap size [13–15], it is difficult to achieve high dioptric power. Since the hydrostatic pressure method requires an external device to apply the pressure, the system is bulky.

In our previous studies [16–20], the electro-wetting method was used for the 2D/3D conversion. This method does not require external devices, has fast response, and is advantageous for securing high diopters because it is not affected by the cell gap like liquid crystals, and it produces a lens shape. The previous studies, however, exhibited relatively limited 3D resolution due to a lens resolution of 60 lines per inch (LPI), and the maximum diopter stayed close to 1500. In this study, we aimed to increase the resolution of the lens to 100 LPI, which is the number that people cannot identify the lens at the mobile viewing distance, and to study the structure needed to obtain the high diopter suitable for this. To satisfy the 100 LPI lens resolution, the thickness of the lens is also required to be reduced as depicted in Fig. 2(b). This means that a structure with a higher diopter is needed because 1500 diopter is insufficient for use in a lenticular lens structure with 100 LPI. If a thick lens with high LPI is used, it will cause a considerable problem in the viewing angle.

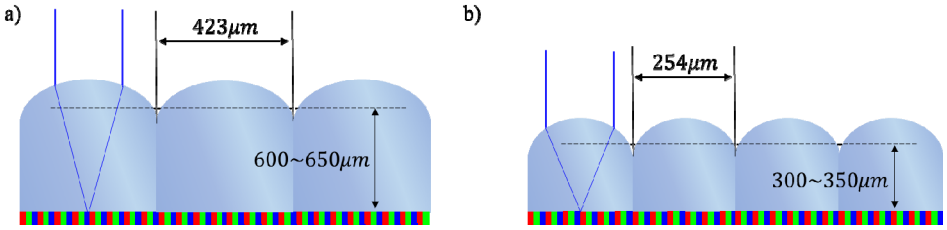

Fig. 2. (a) 60 LPI lenticular configuration requiring diopter near 1500 and (b) 100 LPI lenticular configuration requiring diopter higher than 1500.

2. Basic principle and proposed design

2.1 Electro-wetting lenticular lens

We used the electro-wetting phenomenon in our development of a lenticular type multi-view lens. Plenty of studies about electro-wetting have been done in the field of liquid actuators [21–23], lab-on-a-chip [24–26], and especially liquid lenses [27–30]. We previously developed a method of controlling the lenticular type liquid lens. The new structure suggested here is a liquid-liquid-solid phase bi-convex structure. This structure is particularly effective in electro-wetting driving structure where partitioning walls are essential. For a robust partitioning wall, it needs to occupy a large area of the structure, but it can have a bi-convex structure irrespective of the kind of fluid because the bottom is in the form of a convex lens. It

Optics EXPRESS

also has advantages in multi-view systems where the final focal distance must be the same as the distance to the display, since it can be made thinner than the method of adding multiple layers of lenses. Figure 3 shows the structure of the bi-convex lenticular lens array.

2.2 2D/3D conversion principle

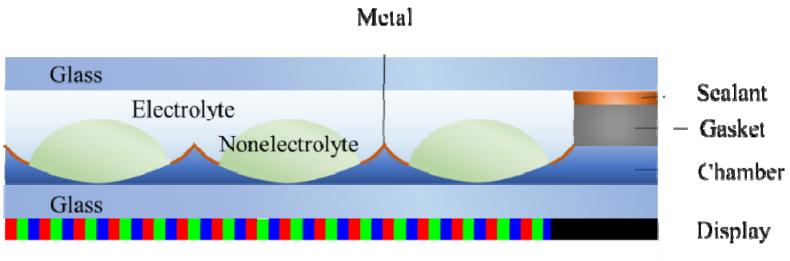

Fig. 3. The structure of the liquid-liquid-solid phases bi-convex structure consists of electrolyte (water), nonelectrolyte (oil) and the lens shaped chamber.

The principle of the electro-wetting approach is based on controlling the contact angle of 3 phases, an electrolyte, nonelectrolyte and a dielectric, on an electrode. The shape of the nonelectrolyte phase can be changed from concave to convex as different voltages are applied. When the combined focal length is infinite, the device is able to export 2D, and the device will export 3D when the combined focal length matches the distance to the display. These conditions are depicted in Fig. 4.

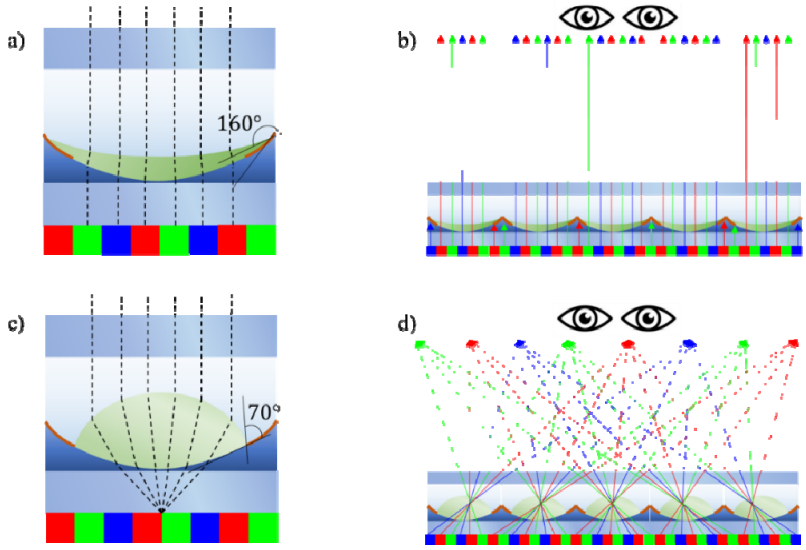

Fig. 4. (a) Hydrophobic state when no voltage is applied, for infinite focal length and (b) the 2D state when the focal length is infinite. (c) Hydrophilic state when the voltage is applied between electrolyte and metal and (d) the 3D state when the focal length matches the distance to the display.

One particular advantage of this structure is that it is not necessary to match the refractive index between the nonelectrolyte and the chamber, as in the previous studies. Therefore, it is only necessary to use a material with a high refractive index. This contributes to a dramatic increase in diopter.

Optics EXPRESS

2.3 Material properties

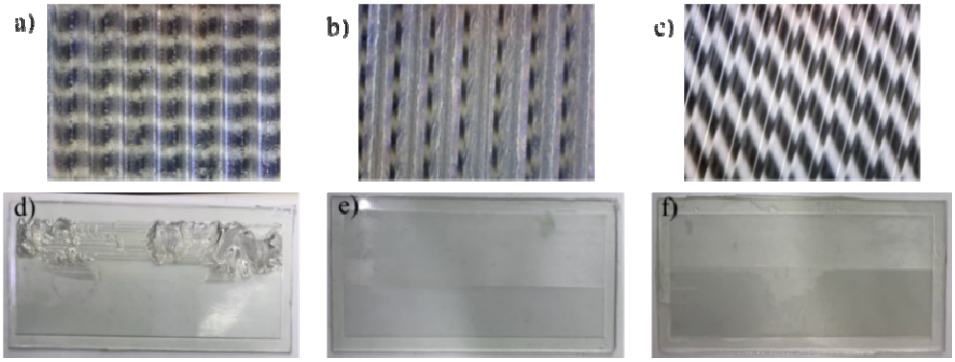

Fig. 5. 1-chloronaphthalene chemical reaction tests with (d) a NOA 85 chamber, (e) a NOA 142 chamber and (f) an ETPTA chamber and their individual microscopic views (a), (b), (c).

To achieve high diopters, 1-chloronaphthalene was selected as the nonelectrolyte phase. The 1-chloronaphthalene has a low gravitational density of 1.194 g $cm^{-3}$and high refractive index of 1.633. These features ensure that a device with 1-chloronaphthalene in the structure can have high diopters without being affected by gravity or impact. However, since the 1-chloronaphtlanene has high chemical reactivity with polymeric materials and acrylic materials, imprinting using PMMA (Poly methyl methacrylate) or PC (Poly carbonate) cannot be used, as in previous studies. Instead, UV curable materials such as the UV adhesive series and ETPTA (Trimethylolpropane ethoxylate triacrylate) were chosen as candidates for the chamber material. The reactivity of 1-chloronaphthalene in the chamber structure was tested using NOA 85 and NOA 142, two representative low-refractive index materials in the UV adhesive series from Norland Products, and ETPTA.

This chemical reactivity experiment lasted for 72 hours, and ETPTA was subsequently selected as the representative candidate. In the case of NOA 85, the chamber was wrinkled and shrunken. With NOA 142, the shape of the chamber was normal, but the shape of the surface became wrinkled. Unlike those cases, ETPTA produced no observable large changes over time, and the surface was smooth. A black striped pattern was placed on the back of the lens to check the curvature and quality of the lens. Figure 5 shows the chemical reaction tests of NOA 85, NOA 142 and ETPTA with 1-chloronaphthalene.

3. Fabrication process

3.1 Mold & chamber fabrication

Because cured ETPTA is a fragile material, it requires a hard substrate such as glass. However, the adhesion force between ETPTA and glass is weak, nickel which has weaker adhesion force to ETPTA than glass is required for ETPTA molding.

Before manufacturing a nickel mold, a commercial PMMA lenticular lens was purchased and used as a master mold to minimize aberrations. For the convex shaped nickel mold, a further intermediate molding process was required. Therefore, a concave NOA 63 slave molding process was added. Then, nickel was electro-plated onto the NOA 63 mold to complete the final mold. Figure 6 shows the commercial PMMA lens, NOA 63 concave mold and final convex nickel mold.

Optics EXPRESS

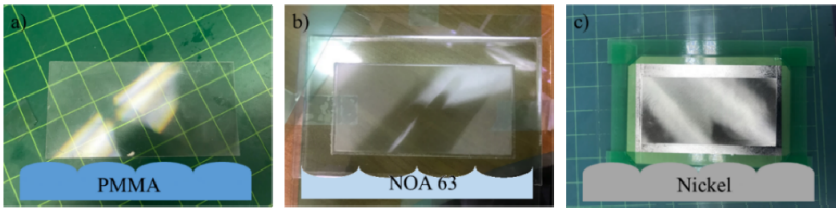

Fig. 6. (a) A commercial PMMA lenticular lens, (b) NOA 63 concave lenticular lens molded by PMMA and (c) a convex electro-plated nickel mold from the NOA 63 concave lens.

In the process of forming the ETPTA chamber on the glass substrate, cracks were found in the chamber during the demolding process due to the weak adhesion force of ETPTA, and NOA 81 was used as the adhesive layer to improve it. Figure 7 depicts the chamber fabrication process. A commercial PMMA lenticular lens has 100 LPI, which means the lens pitch is 254μm and the maximum sag is 69μm. The lenticular sheet was cut to 122 by 64mm with a slanted angle of 52.75 ° to remove the moiré pattern [31]. A urethane release agent was sprayed onto the PMMA sheet to detach NOA 63 easily from the PMMA, and NOA 63 was poured and pressed by a glass plate. After UV curing, the NOA 63 slave mold was fabricated and nickel was electro-plated onto the slave mold. In the process to form the chamber, NOA 81 was selected as the adhesive layer between the ETPTA and glass substrate. The NOA 81 was spin coated on the 300μm thick glass substrate at a speed of 3000rpm for 30 seconds and UV curing was done. Thereafter, ETPTA was poured onto the UV cured NOA 81 layer and pressed by the nickel mold. The ETPTA was cured by UV and finally the ETPTA chamber was fabricated. A slanted evaporation method [20] was used for the electrode deposition. The electrode was 300nm thick silver, and a dielectric layer of 1μm thick parylene C was deposited by chemical vapor deposition method.

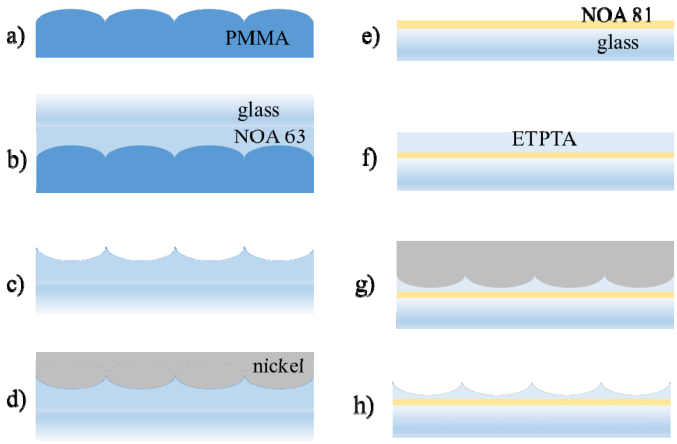

Fig. 7. (a-d) Fabrication process of the nickel mold. (e-h) An ETPTA chamber. (a) A commercial PMMA lenticular lens. (b) NOA 63 was poured onto the PMMA and pressed by glass followed by UV curing. (c) A NOA 63 slave mold was detached. (d) Nickel was electro-plated. (e) NOA 81 was spin coated onto a glass plate and UV curing was done. (f) ETPTA was poured. (g) The nickel mold was pressed and UV curing was done for ETPTA. (h) The ETPTA chamber was detached from the nickel mold.

3.2 Liquid dosing and sealing

Since 1-chloronaphthalene has good adhesion to parylene C, the 1-chloronaphthalene can be injected into the entire chamber in air. The amount of injected 1-chloronaphthalene affects the initial diopter of the lens since the shape of the chamber was a concave lens. Because electro-

Optics EXPRESS

wetting changes the contact angle between the liquid and contact layers, the initial contact angle is determined by the amount of oil injected.

The commercial PMMA lens had a 254μm pitch and 69μm sag, and the ROC (radius of curvature) of the lens was approximately calculated to be 151μm. Assuming the oil does not over flow into the next lens cell, the initial state can be predicted since the contact angle between the oil and ETPTA chamber is 25°. The ROC can be calculated using Eq. (1)

$$ROC = \sqrt{(ROC + sag)^2 + R_L^2} \tag{1}$$

where R_L is the radius of a unit lens. The angle between the horizontal line and the chamber wall can be calculated by Eq. (2)

$$\theta_{WALL} = 90 - \mathrm{a}\tan\left((ROC - sag)/R_L\right) \tag{2}$$

To calculate the diopter induced by the water and oil, the wall angle must be considered in the electro-wetting ROC calculation, as in Eq. (3)

$$ROC_{WO} = R_L / \cos(\theta_{CA} - 90 + \theta_{WALL}) \tag{3}$$

where θ_{CA} is the contact angle of the water phase. Therefore, the diopters can be calculated using focal length Eq. (4)

$$D_{WO} = (n_2 - n_1)/n_1 ROC_{WO} \tag{4}$$

where D_{WO} is a diopter induced by water and oil, n_1, n_2 are the refractive indices of water and oil individually.

Figure 8 shows the initial states after full oil injection and partial oil injection. For the full oil injection state depicted in Fig. 8(a), the initial value of D_{WO} is approximately −1432D. The value of D_{OC} which is the diopter induced by the oil and chamber, can be calculated by the same method and the value is approximately 678D. The synthetic diopter of these two values can be calculated as in Eq. (5)

$$D_{synthetic} = D_{WO} + D_{OC} - dD_{WO}D_{OC} \tag{5}$$

where d is the distance between the center of the two lenses induced by water and oil, and induced by oil and the chamber. When the oil has a concave state, the value of d is negligible. Therefore, the synthetic diopter of the initial state in Fig. 8(a) is −753D, which is a concave lens.

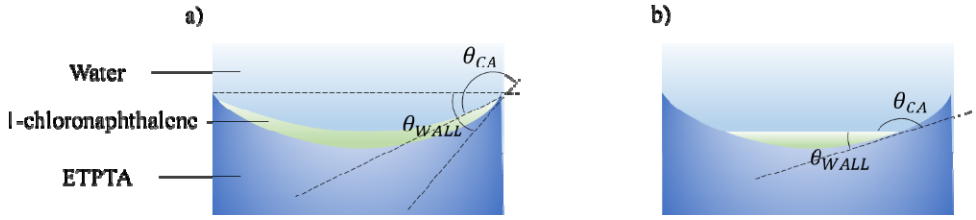

Fig. 8. (a) The state when the oil is fully filled, maintaining the contact angle (b) The plano-convex state formed by a smaller amount of injected oil.

When the oil is partially injected as shown in Fig. 8(b), a plano-convex state can be formed. The diopter in this condition was calculated to be 678D. Therefore, there is a condition between Figs. 8(a) and 8(b) where the diopter becomes 0, and that can be controlled by the amount of oil injection. The volume of 1-chloronaphthalene shown in Fig. 8(a) was then calculated based on the sector width calculation results of the two ROCs

Optics EXPRESS

($ROC_{WO} \cong 210\mu m, ROC_{OC} \cong 151\mu m$). The cross-sectional unit area of 1-chloronaphthalene was 904 μm and the volume in a unit area (254 μm by 254 μm) was approximately 2.3nL. In the same way, the volume of 1-chloronaphthalene shown in Fig. 8(b) was approximately 1.2nL. The initial state of the weak concave was intended and the unit volume of 2nL was determined. The total area of 114mm by 62mm was divided by the unit area, and approximately 230 μL was taken as the initial injection condition.

For uniform liquid dosing, the structure includes an open area that is lower in height than the chamber. Figure 9 shows the open area and liquid flow. After the oil injection, the chamber was covered by ITO (Indium Tin Oxide) coated glass in water.

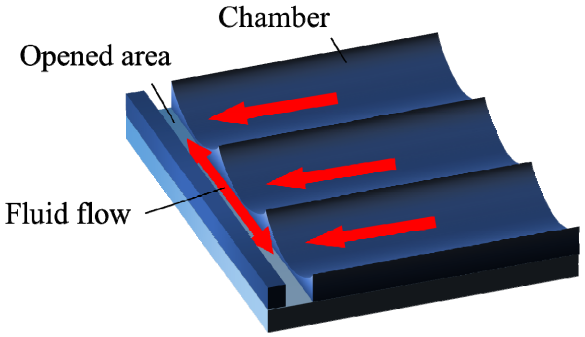

Fig. 9. Liquid flow through the opened area for uniform dosing.

4. Experimental results

Using a Gpro2 mobile phone as a display, the letters 'GIF' were projected through the liquid lenticular sheet. Diopters were measured by measuring the angle between the lenticular sheet and the letter 'I'. Figure 10 shows the measurement setting and operation of concave, flat and convex states. Since the size of the image only changes in the direction horizontal to the lens, the diopter can be found by inverse calculation of the tangential values [17]. The 2D (flat) state can be easily found by controlling the voltage until the 'GIF' letters are projected without any distortion. Since the optimal convex state means the magnification of the lenses is infinite, a very small part of the letters was enlarged, which means the angle is nearly 90°. The diopters depicted in Fig. 10, therefore, were −633D in the initial state, 0D in the flat state and 3030D in the convex state.

In the same way as the diopter measurement, the uniformity was measured by comparing the diopter when a uniform stripe pattern was placed under the lenticular sheet and the same voltage was applied. Figure 11 shows the 3D operation at three arbitrary locations and the Table 1 shows the measured uniformity data. The uniformity was calculated as in Eq. (6)

$$Uniformity = \left(1 - (D_{MAX} - D_{MIN}) / 2 / D_{AVE}\right) \times 100 \quad (6)$$

where $D_{MAX}, D_{MIN}, D_{AVE}$ are maximum, minimum and average diopters respectively.

Optics EXPRESS

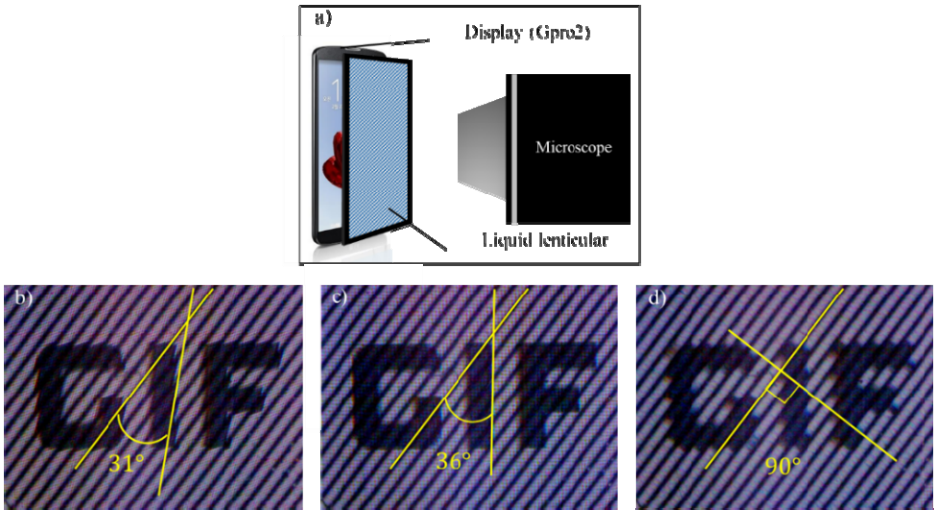

Fig. 10. (a) System setting of the diopter measurement (b) A concave state (c) A flat state (d) A convex state satisfying an optimal focal length.

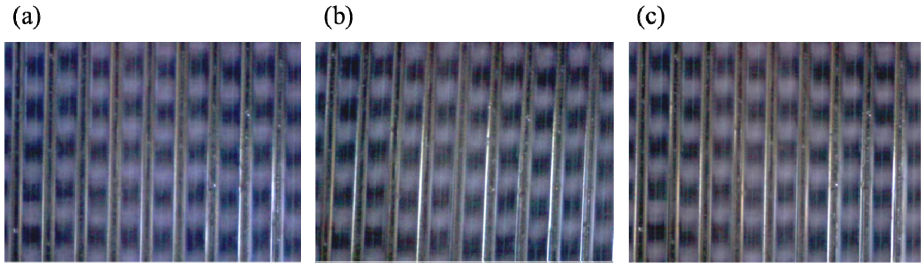

Fig. 11. (a)-(c) An arbitrary three region views for uniformity measurement in 3D mode.

Table 1. Measurement of diopters in Fig. 11 and uniformity calculations

Locations	Measured diopters							Average Diopter	Uniformity
Figure 11(a)	2880	2791	2835	2841	2910	2670	2940	2838	95.2%
Figure 12(b)	2815	2920	2891	2785	2798	2740	2810	2810	96.8%
Figure 13(c)	2855	2910	2885	2912	2912	2894	2923	2923	98.8%

From the results, the uniformity of the liquid was similar locally, but slightly different in the whole area. However, this difference does not have a big effect on the 3D image observation, we conducted 3D observation experiments.

One of the advantages of electro-wetting is that it has a fast response time in a small below the millimeter scale. In order to measure the response speed of the manufactured liquid lenticular sheet, and Nikon 1 J5 high speed camera was used and the response speed was measured by taking a video of 1200FPS (frame per second). This means that the photographing was performed at a speed of 0.833ms per frame. Figure 12 indicates that the operation was completed within about 4 frames. The time until the intentionally tilted stripe pattern changes to the direction perpendicular to the lens as the lens operates was measured. Finally, the operation speed was confirmed to be about 3.33ms.

Optics EXPRESS

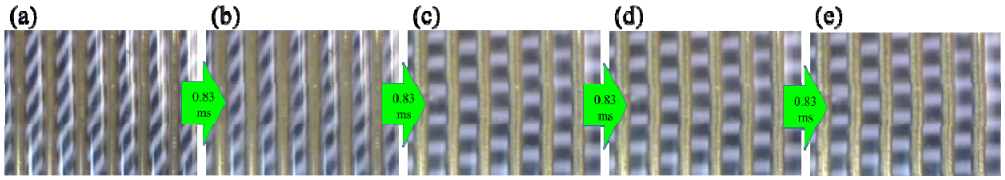

Fig. 12. (a)-(e) 0.833ms interval motion pictures taken with 1200FPS camera.

There was almost no change until the voltage reached 10V, and then it began to change. The flat state was achieved at 18V and the diopter rapidly increased as the voltage rose above the flat state. At the optimal point, the focal lengths of the lenses became the same length as the distance between the center of the lens and the display, which is the best condition for a 3-dimensional multi-view system. From 35V to 45V, the diopter still increased in the stable state, and this can be used as a diopter margin section. After the diopter reached 3425D, the oil began to operate unstably. This phenomenon is induced by the too small contact angle [20]. Therefore, the optimal point for 3D images was the condition where the diopter was 3030D. Figure 13 shows the changes in diopter versus the applied voltage.

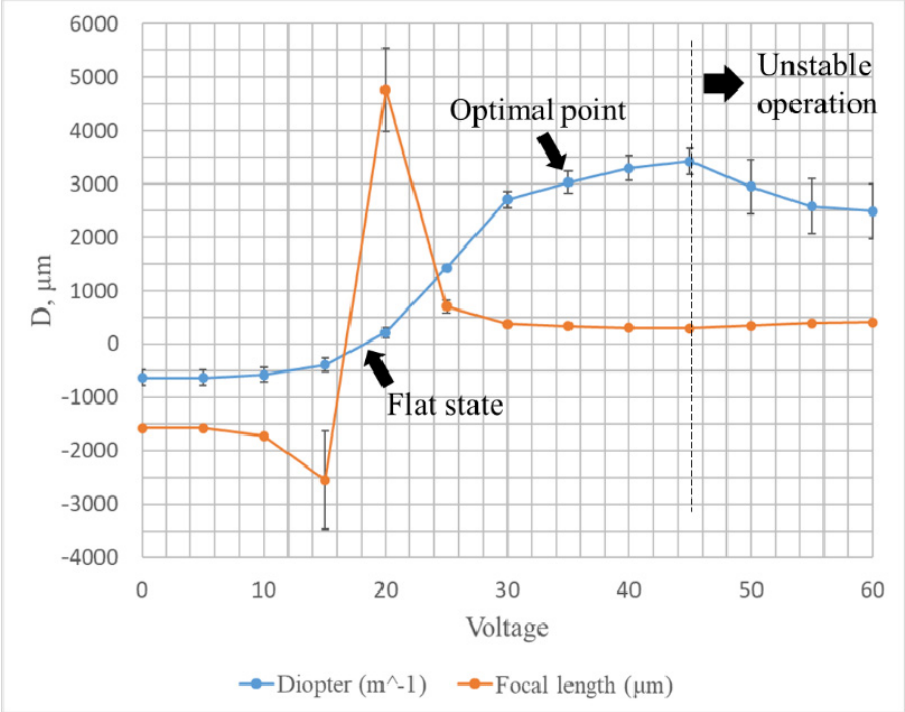

Fig. 13. Diopter and focal length variation by applied voltage.

At 3030D, the crosstalk of the fabricated lenticular lens was tested with 2 views, of a blue image and a red image. The background image was an interlaced pattern of blue and red in each lens and the light intensities of the two colors were measured according to the viewing angle. Figure 14 shows the angular distribution of the color intensities. The crosstalk of a specific viewpoint was calculated using the crosstalk identification equation in multi-view [19]. The crosstalk was minimized to 14.3% at −2° and 22.5% at an average from −10° to 2° which is the blue viewpoint.

Optics EXPRESS

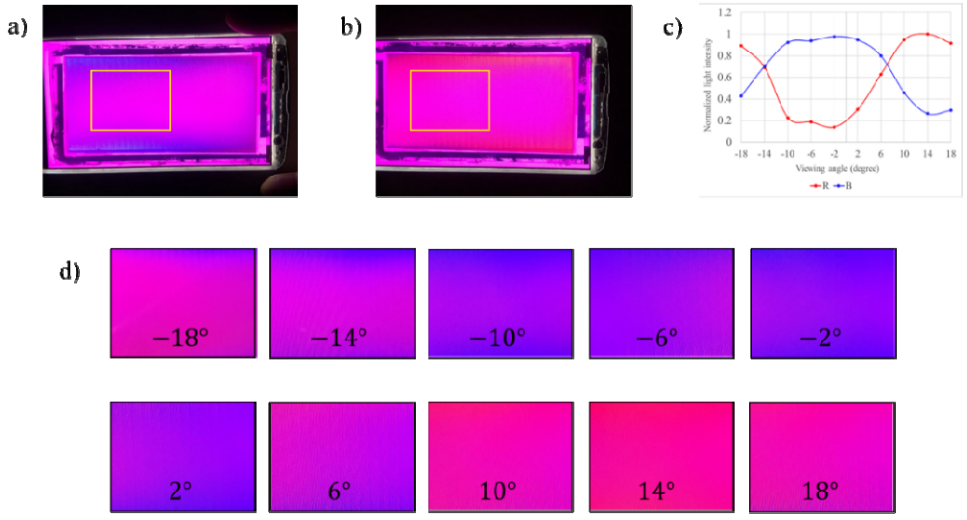

Fig. 14. A 2-view images of blue and red at (a) −14 and (b) 14 and (c) the normalized light intensity. (d) The color distribution of blue and red by the viewing angle.

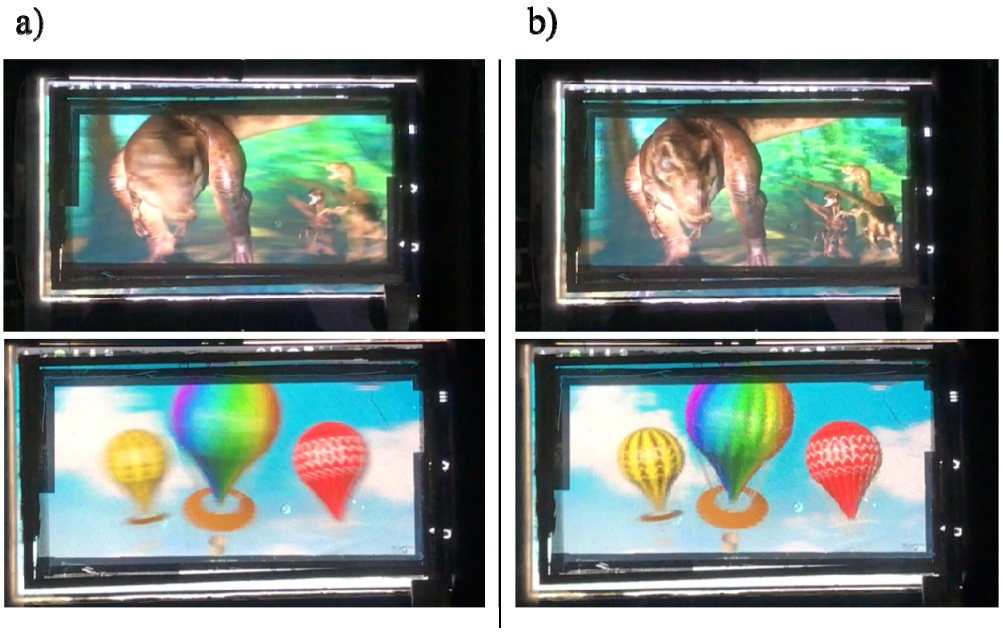

Fig. 15. (a) Multi-view images projected through a 2D state liquid lenticular sheet (b) and 3D state liquid lenticular sheet.

The 3D images shown in Fig. 15 are computer generated multi-view images generated by the 3Ds Max program using the liquid lenticular sheet. Figure 15(b) shows the 3D images at the optimal focal length condition of the display. The image of the head of the Tyrannosaurus, which is a blurred 2D image in Fig. 15(a), shows increased definition when in 3D. The 2D states were conducted at 18V and the 3D state were conducted at 35V. In this experiment, we used a thick dielectric layer to reduce the risk of breakdown during the electro-wetting operation. However, applying our previous work [32] to improve the stability of the dielectric layer using a multi-layer structure, the further lower driving voltage is expected. In addition, because of the electro-wetting principle, the driving power dissipation is very low. Therefore,

Optics EXPRESS

the device can be driven at 3 to 5V by using a boost circuit. Since the LPI is high enough, the dark lines produced by the metal electrodes are not visible to the naked eye.

In order to confirm the motion parallax and the viewing angle of a three-dimensional image, the image was taken by moving the camera left and right at a distance of 30cm from the display. The 3D image was made from 18 viewpoints and among them, 3 viewpoints were taken. Figure 16 shows the 'KAIST' logo is rotating and the head of the Tyrannosaurus moves to the left as the camera taking the 3D image moves to the right. The range of the main zone without image clipping was from −18 ° to 18°.

Fig. 16. Parallax motion of the 3D images viewed at (a) −18 (b) 0 (c) 18 from the display.

5. Conclusion

Lenticular type multi-view technology is advancing and will be commercialized in the near future. The display market is currently in transition from 2D to 3D to meet the demand for 3D imaging. This goal of this study was to develop a 2D and 3D conversion device to satisfy the needs of the 3D display market, and the needs of high-resolution 2D images, focusing on diopter improvement, which is an important factor in the lenticular system.

The key point of this paper is that the chamber has a lens shape and permits the structure to be bi-convex. By using oil with a high refractive index in this structure, the diopter was increased to 3425D and natural quality 3D images were achieved. The range of operating voltage was from 18V to 35V. Since there was a dioptric margin of 395D, the electro-wetting operation was conducted in a stable state.

Optics EXPRESS

Funding

Institute for Information & Communications Technology Promotion (IITP) grant funded by the Korea government (MSIT) (No. 2017-0-01803, Development of Fundamental Technology of Core components for Augmented and Virtual Reality Devices).

References

1. N. A. Dodgson, J. R. Moore, and S. R. Lang, "Multi-view autostereoscopic 3D display," in proceedings of International Broadcasting Convention, **2**. (1999).
2. G. J. Lv, F. Wu, R. Wu, B. C. Zhao, J. Fan, and J. J. Lv, "High resolution parallax barrier 3D display based on a sub display panel with transparent slits," Optik (Stuttg.) **127**(7), 3569–3571 (2016).
3. D. H. Kang, B. S. Oh, J. H. Oh, M. K. Park, H. J. Kim, S. M. Hong, J. H. Hur, J. Jang, S. J. Lee, K. H. Lee, and K. H. Park, "Auto-Stereoscopic TFT-LCD with LC Parallax Barrier on Wire Grid Polarizer," In SID Symposium. Dig. Tech. Pap. **40**(1), 344–347 (2009).
4. T. Peterka, R. L. Kooima, D. J. Sandin, A. Johnson, J. Leigh, and T. A. DeFanti, "Advances in the Dynallax solid-state dynamic parallax barrier autostereoscopic visualization display system," IEEE Trans. Vis. Comput. Graph. **14**(3), 487–499 (2008).
5. H. Isono, M. Yasuda, and H. Sasazawa, "Autostereoscopic 3D display using LCD-generated parallax barrier," Electron. Commun. Jpn. **76**(7), 77–84 (1993).
6. M. Lambooij, K. Hinnen, and C. Varekamp, "Emulating Autostereoscopic Lenticular Designs," IEEE J. Display Technol. **8**(5), 283–290 (2012).
7. Y. Takaki, K. Tanaka, and J. Nakamura, "Super multi-view display with a lower resolution flat-panel display," Opt. Express **19**(5), 4129–4139 (2011).
8. W. X. Zhao, Q. H. Wang, A. H. Wang, and D. H. Li, "Autostereoscopic display based on two-layer lenticular lenses," Opt. Lett. **35**(24), 4127–4129 (2010).
9. I. J. Kim and W. S. Park, "Optimal design of lenticular lens sheet for the 3D display on TFT-LCDs," J. Korean Inst. Electr. Electron. Mater. Eng. **22**(3), 257–261 (2009).
10. H. K. Hong, S. M. Jung, B. J. Lee, H. J. Im, and H. H. Shin, "Autostereoscopic 2D/3D switching display using electric-field-driven LC lens (ELC lens)," in SID Int. Symp. Dig. Tech. Paper, **39**(1), 348–351 (2008).
11. K. C. Heo, S. H. Yu, J. H. Kwon, and J. S. Gwag, "Thermally tunable-focus lenticular lens using liquid crystal," Appl. Opt. **52**(35), 8460–8464 (2013).
12. Y. Limura, T. Teshima, Y. J. Heo, Y. Morimoto, S. Yoshida, H. Onoe, and S. Takeuchi, "Microfluidically tunable lenticular lens," in Proc. 17th Int. Conf. Solid-State Sens., Actuators Microsyst. (TRANSDUCERS EUROSENSORS), 1787–1790, (2013).
13. H. Ren, S. Xu, Y. Liu, and S. T. Wu, "Switchable focus using a polymeric lenticular microlens array and a polarization rotator," Opt. Express **21**(7), 7916–7925 (2013).
14. H. Urey, K. V. Chellappan, E. Erden, and P. Surman, "State of the art in stereoscopic and autostereoscopic displays," Proc. IEEE **99**(4), 540–555 (2011).
15. H. Ren and S. T. Wu, "Adaptive liquid crystal lens with large focal length tunability," Opt. Express **14**(23), 11292–11298 (2006).
16. C. Kim, J. Kim, D. Shin, J. Lee, G. Koo, and Y. H. Won, "Electrowetting lenticular lens for a multi-view autostereoscopic 3D display," IEEE Photonics Technol. Lett. **28**(22), 2479–2482 (2016).
17. J. Lee, J. Kim, C. Kim, D. Shin, G. Koo, J. H. Sim, and Y. H. Won, "Improving the performance of an electrowetting lenticular lens array by using a thin polycarbonate chamber," Opt. Express **24**(26), 29972–29983 (2016).
18. D. Shin, J. Kim, C. Kim, G. H. Koo, J. H. Sim, J. Lee, and Y. H. Won, "Effect of oil on an electrowetting lenticular lens and related optical characteristics," Appl. Opt. **56**(7), 1886–1892 (2017).
19. J. Lee, J. Kim, G. Koo, C. Kim, D. Shin, J. H. Sim, and Y. H. Won, "Analysis and reduction of crosstalk in the liquid lenticular lens array," IEEE Photonics J. **9**(39), 1943–2655 (2017).
20. J. Kim, J. Lee, C. Kim, D. Shin, G. Koo, and Y. H. Won, "Optimization of a liquid lenticular system for 2D and 3D conversion," IEEE Photonics Technol. Lett. **29**(18), 1540–1543 (2017).
21. Y. Y. Lin, E. R. F. Welch, and R. B. Fair, "Low voltage picoliter droplet manipulation utilizing electrowetting-on-dielectric platforms," Sens. Actuators B Chem. **173**, 338–345 (2012).
22. J. H. Song, R. Evans, Y. Y. Lin, B. N. Hsu, and R. B. Fair, "A scaling model for electrowetting-on-dielectric microfluidic actuators," Microfluid. Nanofluidics **7**(1), 75–89 (2009).
23. M. G. Pollack, R. B. Fair, and A. D. Shenderov, "Electrowetting-based actuation of liquid droplets for microfluidic applications," Appl. Phys. Lett. **77**(11), 1725–1726 (2000).
24. A. Schultz, I. Papautsky, and J. Heikenfeld, "Investigation of laplace barriers for arrayed electrowetting lab-on-a-chip," Langmuir **30**(18), 5349–5356 (2014).
25. S. W. Walker and B. Shapiro, "Modeling the fluid dynamics of electrowetting on dielectric (EWOD)," J. Micromech. Syst. **15**(4), 986–1000 (2006).
26. J. Zeng and T. Korsmeyer, "Principles of droplet electrohydrodynamics for lab-on-a-chip," Lab Chip **4**(4), 265–277 (2004).

Optics EXPRESS

27. L. Li, C. Liu, H. Ren, and Q. H. Wang, "Optical switchable electrowetting lens," IEEE Photonics Technol. Lett. **28**(14), 1505–1508 (2016).
28. S. Terrab, A. M. Watson, C. Roath, J. T. Gopinath, and V. M. Bright, "Adaptive electrowetting lens-prism element," Opt. Express **23**(20), 25838–25845 (2015).
29. N. R. Smith, L. Hou, J. Zhang, and J. Heikenfeld, "Fabrication and demonstration of electrowetting liquid lens arrays," J. Disp. Technol. **5**(11), 411–413 (2009).
30. B. H. W. Hendriks, S. Kuiper, M. A. J. Van As, C. A. Renders, and T. W. Tukker, "Electrowetting-based variable-focus lens for miniature systems," Opt. Rev. **12**(3), 255–259 (2005).
31. Z. Zhuang, P. Surman, L. Zhang, R. Rawat, S. Wang, Y. Zheng, and X. W. Sun, "Moire-reduction method for slanted-lenticular-based quasi-three-dimensional displays," Opt. Commun. **381**, 314–322 (2016).
32. A. Grisatya and Y. H. Won, "Multi-layer insulator for low voltage and breakdown voltage enhancement in electrowetting-on-dielectric," Proc. SPIE **8987**, 89871S (2014).